

ELECTROSTATIC LOFTING OF DUST GRAINS FROM THE SURFACES OF THEBE AND AMALTHEA

N. Borisov^{1,2}, H. Krüger²

¹IZMIRAN, 108840, Moscow, Troitsk, Russia

²MPI for Solar System Research, 37077, Göttingen, Germany

Abstract

Energetic electrons from the inner radiation belt provide significant electric charging of the surfaces of Jupiter’s moons Thebe and Amalthea whose orbits are located within this radiation belt. We estimate theoretically the electric fields in the vicinity of the polar regions of Thebe and Amalthea and argue that these fields are sufficient for lofting of micron and submicron-sized dust grains from the surfaces of the moons. Thus, the lofting of charged dust grains in the electric fields can be considered as an additional source supplying dust to the gossamer rings in addition to dust ejection by micrometeoroid impacts onto the moons’ surfaces. The suggested mechanism can explain qualitatively some peculiarities of the dust grain distributions within the gossamer rings.

Keywords: Electrostatic dust levitation, Jupiter gossamer ring, Amalthea, Thebe.

1 Introduction

Jupiter has a highly structured dust ring system that extends along the planet’s equatorial plane. It consists of the main ring, the halo, two gossamer rings and the Thebe extension (Burns, 1984; Showalter et al., 1987; Burns et al., 2004). This dust system was investigated by the space missions Voyager 1/2, Galileo, Cassini and New Horizons (Smith et al., 1979; Owen et al., 1979; Ockert-Bell et al., 1999; Porco et al., 2003; Burns et al., 2004; Showalter et al., 2007; Throop et al., 2016) and also by telescopes in space (Hubble) and from the Earth (Keck) (de Pater et al., 1999, 2008; Showalter et al., 2008).

The main ring is located between $1.72R_J$ and $1.806R_J$ from Jupiter, where R_J is the radius of Jupiter $R_J = 71,492$ km. This ring has an optical depth $\tau \geq 10^{-6}$ and a thickness perpendicular to Jupiter’s equatorial plane of approximately 30 – 100 km. Its radial extension is of the order of 6000 km. Interior to the main ring the halo has a rather wide ($\sim 2 \cdot 10^4$ km) and thick ($\sim 10^4$ km) structure with an optical depth of $\tau \sim 10^{-6}$, similar to that of the main ring. Jupiter’s gossamer ring system was detected out to $3.5R_J$ from the planet on optical images and further beyond with in-situ detections, see, e.g. Showalter et al. (2008). Two small moons, Amalthea and Thebe, orbiting Jupiter within the ring region (at $2.5R_J$ and $3.1R_J$ distance from the planet), are generally considered as the major dust sources feeding the gossamer rings via the ejection of particles released due to bombardment of the surfaces of these moons by micrometeoroids.

The Amalthea ring is brighter and narrower than the Thebe ring. It is situated between the main ring and the orbit of the moon Amalthea. This ring has a slightly triangular shape when viewed edge-on and its optical depth is $\tau \sim 10^{-7}$. The dust particles detected in the ring have sizes of $0.5 - 2.5 \mu\text{m}$ (Krüger et al., 2009). The Thebe ring is broader and fainter than the Amalthea ring, with an optical depth $\tau \sim 3 \cdot 10^{-8}$. It terminates at the orbit of Thebe. The sizes of dust particles in this ring are similar to those measured within the Amalthea ring. Outside Thebe’s orbit there is one more (even fainter) structure which is known as the Thebe extension. The distribution of dust in the gossamer rings has some peculiarities: The thickness of these rings is approximately determined by vertical excursions of the corresponding moons during their orbital motion around Jupiter, and the ring’s upper and lower edges are much brighter than their central parts. In both rings the height integrated concentration of dust grains has its maximum just interior to the corresponding moon’s orbit.

It is commonly believed that dust forming the gossamer rings is supplied exclusively due to continuous bombardment by micrometeoroids onto the surfaces of Thebe and Amalthea (Krivov et al., 2002; Dikarev et al., 2006). On the other hand, electric charging of dust in planetary rings has also been considered (Graps et al., 2008). It is usually accepted that dust grains lofting from the surfaces of cosmic objects without an ionosphere (e.g., the Moon and asteroids) is caused by the electric forces due to surface charging of dust grains located on the surface, see, e.g. Lee (1996); Horányi et al. (1998); Colwell et al. (2005). The dust surface charge is provided by photoelectron emission caused by solar UV radiation and plasma impacting the grain surface. Such a mechanism can be efficient if electric forces acting on dust grains near the surface are strong enough to overcome gravity and adhesion (Hartzell and Scheeres, 2011; Hartzell et al., 2013; Hartzell and Scheeres, 2013; Kimura et al., 2014; Wang et al., 2016). On the surfaces of objects without an ionosphere, strong electric fields can be formed on uneven surfaces near the terminator and at the un-illuminated side because the fluxes of solar wind electrons and protons that hit the surface are not the same (Borisov and Mall, 2006).

Jupiter has a strong magnetosphere which prevents the solar wind plasma from penetrating into it. The plasma composition of Jupiter’s inner magnetosphere is complicated. The plasma in Jupiter’s inner magnetosphere was modelled based on the Pioneer and Voyager data provided by Divine and Garrett (1983). Later on, this model was improved with results from more recent space missions (Garrett et al., 2005). Unfortunately, up to now only a few plasma observations are available for the inner magnetosphere of Jupiter. As a consequence, exact plasma parameters in this region are still not well-known, however, the Juno mission (Bolton, 2010) that has recently arrived at Jupiter will help to solve this problem in the future. Different plasma populations were identified in Jupiter’s inner magnetosphere. They are variable in time, so that existing models can represent only an averaged distribution. First, it is thermal plasma approximated by the Boltzmann distribution with some finite temperature. Second, energetic electrons and protons that form the radiation belts exist in the inner magnetosphere. Up to now only the fluxes of electrons with energies $W \geq 160 \text{ keV}$ and protons with energies above $W \approx 1.2 \text{ MeV}$ were measured in the inner radiation belt, (see, e.g., Khurana et al., 2004).

The fluxes of energetic electrons are very large. Depending on the model, in the vicinity of Thebe or Amalthea, they can be of the same order of, or even exceed, the fluxes of thermal electrons. The probability that such energetic electrons impact micron-sized or smaller dust particles in the gossamer rings is negligible, hence charging of small dust particles due to energetic electrons with energies exceeding $W > 100$ keV can be neglected. At the same time such energetic electrons contribute to the charging of the moons' surfaces, leading to the formation of strong surface electric fields.

Up to now the role of surface charging in dust grains lofting from Thebe and Amalthea has not been investigated. The aim of the present paper is to investigate theoretically the electric fields near the surfaces of these two jovian moons (in particular in their polar regions) due to the charging by the fluxes of electrons and protons. As the magnetized electrons and protons propagate along the magnetic field lines, their fluxes to the unit square on the surface are proportional to $\cos \theta$ (where θ is the angle between the magnetic field and the normal to the surface). Such fluxes onto the surface reach their maximum values in the vicinity of the polar regions where the angle θ is small. Hence, the strongest negative potential on the surface is expected in the polar regions. This provides more favourable conditions for charged particles to leave the moons. Simultaneously, the solar UV radiation acts only on the sunlit side and its flux is practically tangential to the surface in the polar regions. So, it does not produce any significant charging there. Below we estimate the sizes of dust grains that can be lofted from the surfaces by the predicted electric fields.

2 Basic equations

First we need to introduce the distribution of plasma components in the inner radiation belt of Jupiter. As we concentrate on the surface charging and dust grain lofting from Thebe and Amalthea we are interested in the plasma distribution at the radial distances $\approx 3.1 R_J$ (orbit of Thebe) and $\approx 2.5 R_J$ (orbit of Amalthea). As mentioned above, parameters of the inner magnetosphere of Jupiter are still not well-known. Nevertheless, based on the existing models we introduce the Boltzmann distribution which describes thermal electrons:

$$F_e^{(th)} = \frac{N_{e,th}}{(\sqrt{\pi}V_{e,th})^3} \exp\left(-\frac{v^2}{V_{e,th}^2}\right) \quad (1)$$

and thermal ions

$$F_i^{(th)} = \frac{N_{i,th}}{(\sqrt{\pi}V_{i,th})^3} \exp\left(-\frac{v^2}{V_{i,th}^2}\right). \quad (2)$$

Here $N_{e,th}$, $N_{i,th}$ are the concentrations of electrons and ions, and $V_{e,th}$, $V_{i,th}$ are their thermal velocities. The temperatures are assumed to be equal to each other $T_{e,th} = T_{i,th} = T_{th}$. Note that in the inner magnetosphere the most abundant ions are oxygen O^+ ($\sim 20\%$) and sulphur S^+ ($\sim 70\%$) instead of protons.

The distribution of energetic electrons and protons in the radiation belt can be modeled as a power-law distribution (it is often called a kappa distribution) (Divine and Garrett, 1983):

$$F_\alpha(W) = N_{\alpha,h} \left(\frac{m_\alpha}{2\pi W_{0,\alpha}} \right)^{3/2} \frac{\Gamma(\kappa + 1)}{\kappa^{3/2} \Gamma(\kappa - 1/2) (1 + W/\kappa W_{0,\alpha})^{\kappa+1}}. \quad (3)$$

Here, $N_{\alpha,h}$ with $\alpha = e, i$ are the concentrations of hot electrons and protons in the radiation belt, $W_{0,\alpha}$ is the characteristic energy. Parameters $W_{0,\alpha}$ and κ should be chosen such that they represent more or less accurately the energy distributions of electrons and protons experimentally measured in the radiation belt.

Our aim is to provide only estimates of dust charging. So, we shall use rather simple power-law distributions that make it possible to obtain the results analytically. Different electron distributions exist in the radiation belts. Among them are the so-called loss-cone distribution and the pancake distribution. The loss-cone distribution corresponds to the case when for a given energy, W , in the equatorial plane the transverse velocity of electrons is much smaller than the longitudinal velocity. Indeed, energetic electrons in the radiation belt bounce between the reflection points where the magnetic field reaches such high values that the longitudinal velocity becomes equal to zero. As in the magnetic field for strongly magnetized electrons the magnetic moment $\mu = v_\perp^2/2H$ is conserved, the longitudinal velocity is presented in the form $v_z^2 = 2(W/m - \mu H(z))$. It follows from this relation that for a given energy the longitudinal velocity decreases while electrons move along the magnetic field line towards the poles. At the same time the longitudinal velocity reaches its maximum value near the equator. In the theoretical analysis for such a distribution of electrons the following model is often used:

$$F_e^{(h)} = \frac{24}{\pi^2} N_{e,h} \frac{v_\perp^2 V_{e,h}^3}{(v_z^2 + v_\perp^2 + V_{e,h}^2)^4}. \quad (4)$$

Here $N_{e,h}$ is the concentration of energetic electrons, v_z, v_\perp are their velocities along and across the magnetic field line, and $V_{e,h}$ is the characteristic velocity of energetic electrons. If we present $v_\perp = v \sin \alpha$ (where α is a pitch angle) it becomes clear that the distribution (4) has a maximum for large pitch angles $|\alpha| \approx \pi/2$. The corresponding concentration $N_{e,h}$ we present in the form $N_{e,h} = \eta_e N_{e,th}$, where $\eta_e \ll 1$ is a relative concentration of energetic electrons with respect to thermal electrons. Note that in the model by Garrett et al. (2005) a very strong dependence on the pitch angle $\propto \sin^4 \alpha$ was introduced in addition to the isotropic distribution (Levin et al., 2001). In our rather crude estimates we shall use the distribution (4) which qualitatively describes the anisotropy of the electron distribution.

Another possible distribution of electrons is a pancake distribution. According to the analysis of the synchrotron emission in the inner radiation belt of Jupiter at small L-shells ($L < 2$) the distribution of energetic electrons near the equator has some fraction which can be described as a pancake distribution, see, e.g. Garrett et al. (2005). The

peculiarity of this distribution is that the maximum corresponds to small pitch angles. Such a distribution can be modelled analytically as the following:

$$F_e^{(h)} = \frac{48}{\pi^2} N_{e,h} \frac{v_z^2 V_{e,h}^3}{(v_z^2 + v_\perp^2 + V_{e,h}^2)^4}. \quad (5)$$

For $v_z = v \cos \alpha$ the distribution (5) indeed has its maximum at small pitch angles. As the moons Amalthea and Thebe orbit Jupiter at larger L-shells, such a pancake distribution will be absent in our calculations.

For energetic protons in the radiation belt we introduce the distribution:

$$F_i^{(h)} = \frac{16\eta_i N_0}{\pi^2} \frac{v^2 V_{i,h}^3}{(v^2 + V_{i,h}^2)^4}. \quad (6)$$

Contrary to eq. (3) our model (6) describes qualitatively the decrease of the proton distribution not only for high energies $v^2 \gg V_{i,h}^2$ but also for small energies $v^2 \ll V_{i,h}^2$. It looks reasonable because the distribution of energetic protons should decrease for small enough energies. To preserve the quasineutrality of the plasma we assume that $N_{e,th} = N_0$, $N_{i,th} = (1 + \eta_e - \eta_i)N_0$. Parameters N_0 , η_e , η_i , $v_{e,h}$, $v_{i,h}$ are to be determined from the experimental data.

We need to take into account the emission of secondary electrons from the moon's surface due to bombardement by fast electrons because secondary electrons can make a significant contribution to surface charging (Whipple, 1981). The amount of newly created secondary electrons at the surface is determined by the energy distribution of primary electrons hitting the surface and the yield $\delta(W)$:

$$\delta(W) \approx 7.4\delta_m \frac{W}{W_m} \exp \left[-2 \left(\frac{W}{W_m} \right)^{1/2} \right], \quad (7)$$

where $W = mv^2/2$ is the energy of a primary electron, δ_m is a maximum yield, and W_m is the energy that corresponds to the maximum yield (Whipple, 1981; Horányi, 1993). Parameters δ_m , W_m depend on the material of the surface. For a thermal distribution of primary electrons (see, eq. 1) the amount of secondary electrons in the range of energies $W, W + dW$ is

$$\frac{dN_{e,sec}^{(th)}}{dW} = \frac{2}{\sqrt{\pi}} \delta(W) N_{e,th} \exp \left(-\frac{W}{W_{e,th}} \right) \frac{\sqrt{W}}{W_{e,th}^{3/2}}. \quad (8)$$

Here $W_{e,th} = mV_{e,th}^2/2$ is the thermal energy. Similarly, we present the production of secondary electrons by energetic primary electrons (eq. 4):

$$\frac{dN_{e,sec}^{(h)}}{dW} = 8\delta(W) N_{e,h} W_{e,h}^{3/2} \frac{W_\perp \sqrt{W}}{(W + W_{e,h})^4}, \quad (9)$$

where $W_{e,h} = mV_{e,h}^2/2$. The energy distribution of the secondary electrons is usually modelled as a Boltzmann distribution with a low temperature $T_s \sim 2\text{eV}$. Later on, for simplicity, we assume that all secondary electrons are born with the same velocity $v_s = (2T_s/m)^{1/2}$. The equations presented above make it possible to estimate the stationary electric potential near the surface of the moon. Only a yet unknown electric potential φ should be introduced in the distribution functions of electrons and ions near the surfaces of the moons.

3 Calculation of the electric potential on the surface of a large body in a magnetized plasma

We would like to estimate the electric potential on the surface of a given moon in the vicinity of its polar region. Here, we assume Jupiter's magnetic field lines to be orthogonal to the surface. The Larmor radii of (not only thermal but also energetic) ions are much smaller than the sizes of Thebe and Amalthea. Therefore, it is possible to define two planes. The first one is Jupiter's equatorial plane, and the orbital planes of both moons are very close to this plane. The second plane corresponds to the magnetic equator of Jupiter. The angle between these two planes is $\beta \approx 10^\circ$. Suppose that at the magnetic equator far from the moon (where the electric potential tends to zero, i.e. $\varphi \approx 0$) the distribution functions of charged particles are given by equations presented in Section 2. Note that we use non-relativistic expressions for the magnetic moment and the energy of electrons. Electrons become relativistic if their kinetic energies exceed $W \approx mc^2 \approx 0.5\text{MeV}$. For smaller energies electrons can be considered as non-relativistic. But even for electrons with energies $W \sim 1\text{MeV}$ relativistic corrections are rather moderate and can be neglected for our estimates.

The magnetic field H for a given L-shell changes along the magnetic field line. We therefore use the invariant parameters μ and $w = v_\perp^2 + v_z^2$ instead of velocities v_\perp and v_\parallel . The element of phase space in these parameters takes the form

$$2\pi v_\perp dv_\perp dv_z = \pi \frac{dw H d\mu}{\sqrt{w - H\mu}}. \quad (10)$$

As the magnetic field grows towards the poles, the distribution of charged particles (first of all electrons) along the magnetic field line changes. Indeed, electrons with small longitudinal velocities are reflected where $w = 2\mu H$. But in our case this effect is small. Indeed, in the dipole magnetic field for a given L-shell and the moon's orbital inclination with respect to the magnetic equator of $\beta = 10^\circ$, the growth of the magnetic field is only $\approx 12\%$ with respect to the value at the equator. This means that electrons with a pitch angle at the magnetic equator $\alpha \leq 70^\circ$ are able to reach a given moon (Thebe or Amalthea). But these electrons deposit their charge on the moon's surface only if the longitudinal energy at the magnetic equator $mv_z^2/2$ exceeds the potential energy of the surface $|e\varphi_s|$. Taking into account that our estimates are rather simple (first, because our present knowledge of the electron and ion distributions is not sufficient and second,

the real magnetic field deviates from a dipole field) small variations of the magnetic field strength along the magnetic field line at the angles $\beta \leq 10^\circ$ can be neglected.

Near the surface of the moon the electric potential φ tends to equalize the fluxes of electrons and ions hitting the surface. Due to this, the variable w in the distribution of electrons changes to $w - 2e\varphi/m$. In this paper we present rather simple estimates of the surface charging and assume that the electric and magnetic fields vary only in one direction (along the magnetic field line). Therefore, we introduce the system of coordinates in which the z-axis is directed along the magnetic field, and the x-axis is in the radial direction. With the help of the model distributions presented in Section 2 and taking into account that the electric field varies only along the z-axis we can calculate the electric charge that reaches the surface on a unit square per second. Note that the angular velocity with which the magnetosphere of Jupiter rotates deviates from the orbital angular velocities of the moons Thebe and Amalthea. This leads to the radial electric field, the so-called $\mathbf{v} \times \mathbf{B}$ field. According to our estimates, this field is much smaller than the polarization electric field caused by the charging of the surface and to a first order approximation it does not influence the lofting of dust grains. At the same time this electric field determines the dynamics of dust particles on rather long time scales after they leave the vicinity of the surface.

Under stationary conditions the electric charge that electrons carry to the unit square on the surface should be equal to the electric charge that is carried by ions. From this relation the electric potential on the surface φ_s is obtained. As the non-disturbed flux of electrons is larger than the flux of ions, the electric potential φ_s should be negative. This means that electrons are retarded while ions are accelerated towards the surface.

We shall estimate the fluxes of electrons and ions that deposit electric charges on the surface of the moons at their polar regions where the z-axis is assumed to be normal to the surface. The flux of thermal electrons along the z-axis is

$$P_{e,z}^{(th)} = \frac{N_0 V_{e,th}}{2\sqrt{\pi}} \exp\left(\frac{e\varphi_s}{T_{th}}\right). \quad (11)$$

Similarly, the flux of thermal ions is

$$P_{i,z}^{(th)} = \frac{(1 + \eta_e - \eta_i) N_0 V_{i,th}}{2\sqrt{\pi}}. \quad (12)$$

Note that this flux does not depend on the electric potential φ . The reason for this is that we consider the 1-D case assuming that the electric field is directed only along the z-axis. In this model the flux of propagating ions is conserved and, hence, it does not depend on the electric potential. The reason why we can consider the one-dimensional case as an approximation is that protons are strongly magnetized in the inner magnetosphere of Jupiter. Hence, they are coupled to the magnetic field lines. The Larmor radius of the thermal ions is of the order of $\rho_{Hi}^{(th)} \leq 100$ m and for energetic protons it is $\rho_{Hi}^{(h)} \approx 2.5$ km. These scales are much smaller than the size of the polar zone within which the electric potential can be considered as a constant.

The flux of energetic electrons with the distribution function (4) is

$$P_{e,z}^{(h)} = \frac{2\eta_e N_0 V_{e,h}}{\pi \left(1 - \frac{e\varphi}{W_{e,h}}\right)}, \quad (13)$$

where $V_{e,h} = \sqrt{\frac{2W_{e,h}}{m}}$. To determine the coefficient η_e we need to equate the model flux of energetic electrons within some energy channel $\Delta P_{e,z}^{(h)}$ far away from the surface with the measured one

$$\Delta P_{e,z}^{(h)} = \frac{6}{\pi} \eta_e N_0 w_{e,h}^{3/2} \int_{w_1}^{w_2} \frac{x^2}{(x + w_{e,h})^4} dx, \quad (14)$$

where $w_1 = v_{min}^2$, $w_2 = v_{max}^2$ determine the energy channel within which the flux of energetic electrons is measured, $w_{e,h} = 2W_{e,h}/m$.

The flux of energetic ions with the distribution function (6) is easily calculated:

$$P_{i,z}^{(h)} = \frac{\eta_i N_0 V_{i,h}}{48\pi}. \quad (15)$$

The parameter η_i that enters eq. (15) can be determined in the same way as for electrons.

The fluxes of the secondary electrons from the surface of the moon caused by thermal and energetic electrons are obtained with the help of eqs. (8) and (9). The yield $\delta(w)$ has its maximum at rather moderate energies W_m , which are much smaller than the typical energy of energetic electrons. Also we suppose (it will be confirmed by calculations) that the electric potential on the surface exceeds significantly the energy W_m , that is $|e\varphi_s| \gg W_m$. In this case the flux of the secondary electrons produced by energetic electrons takes the form

$$P_{e,z}^{(sec,h)} \approx \frac{4N_{e,h} V_{e,h}^3 v_{s,z}}{\sqrt{\frac{-2e\varphi_s}{m}} (w_{e,h} - \frac{2e\varphi_s}{m})^4} \int_0^\infty \delta(w) w^2 dw. \quad (16)$$

The flux of the secondary electrons that correspond to the thermal primary electrons takes the form

$$P_{e,z}^{(sec,th)} \approx 9.1 \delta_m v_{s,z} N_0 \frac{W_{e,th}}{W_m} \exp\left(\frac{e\varphi_s}{T_{th}}\right), \quad (17)$$

where $v_{s,z}$ is the z-component of the velocity of the secondary electrons ($v_{s,z} \approx \frac{2}{\pi} v_s$ for electrons with equal probability emitted from the surface in different directions). Suppose that the surfaces of both moons are covered with regolith which has very small electric conductivity (it can be considered almost an insulator). In this case the stationary electric potential on the surface is determined by the local relation

$$P_{e,z}^{(th)}(\varphi_s) + P_{e,z}^{(h)}(\varphi_s) - P_{e,z}^{(sec)}(\varphi_s) = P_{i,z}^{(th)} + P_{i,z}^{(h)}. \quad (18)$$

The flux of electrons produced by the solar UV radiation is absent in eq (18). As it was mentioned in the Introduction the role of this radiation in charging of the polar regions is negligible even on the sunlit side. After the substitution of the fluxes of electrons and ions presented above we are in a position to find from eq. (18) the surface electric potential. This will be done in the next section.

4 Estimates of the surface electric potentials for Thebe and Amalthea

In order to find the value of the electric potential on the surface from eq. (18) we need to provide concrete values for the input parameters. According to Divine and Garrett (1983, see their Fig. 10), the concentration of thermal plasma at the orbit of Thebe is $N_0(3.1R_J) \approx 50 \text{ cm}^{-3}$, and at the orbit of Amalthea it is $N_0(2.5R_J) \approx 100 \text{ cm}^{-3}$. The temperature of thermal plasma is $T_e = T_i = 46 \text{ eV}$. Note that the main thermal ions in the inner magnetosphere are not protons but heavy ions O^+ and S^+ . Available experimental data show that the strongest omnidirectional flux of energetic electrons corresponds to the energy channel $0.19 \text{ MeV} < W < 0.26 \text{ MeV}$ and for protons it corresponds to the channel $1.2 \text{ MeV} < W < 2.15 \text{ MeV}$. For the orbit of Thebe the flux of electrons in a given channel is $\Delta P_e^{(h)} \approx 6 \cdot 10^8 \text{ cm}^{-2}\text{s}^{-1}$, for the orbit of Amalthea it is an order of magnitude less $\Delta P_e^{(h)} \approx 6 \cdot 10^7 \text{ cm}^{-2}\text{s}^{-1}$. The flux of ions in a given channel for the orbit of Amalthea is $\Delta P_i^{(h)} \approx 6 \cdot 10^6 \text{ cm}^{-2}\text{s}^{-1}$, which is slightly less than the value for Thebe: $\Delta P_i^{(h)} \approx 10^7 \text{ cm}^{-2}\text{s}^{-1}$. We shall use these fluxes to determine the coefficients η_e and η_i . The parameters for secondary electrons (maximum yield δ_m and the corresponding energy W_m) vary significantly depending on the surface material. The energy W_m can be of the order of approximately $100 - 1000 \text{ eV}$ while the maximum yield δ_m varies from less than unity up to 30. In our calculations we take $W_m = 200 \text{ eV}$ and several different values of δ_m .

We shall use the model loss-cone distribution (4) for energetic electrons in the vicinity of Thebe and Amalthea. Comparison with the experimental data makes it possible to estimate the fraction of energetic electrons (4) $\eta_e \approx 4 \cdot 10^{-3}$ and ions (6) $\eta_i \approx 0.04$ for Thebe's orbit. After the substitution of fluxes eq. (18) takes the form

$$(12 - 5.3\delta_m) \exp\left(\frac{e\varphi_s}{T_{th}}\right) + \frac{2.8}{1 - \frac{e\varphi_s}{W_{e,h}}} - \frac{4 \cdot 10^{-5}\delta_m}{\left(-\frac{e\varphi_s}{W_{e,h}}\right)^{1/2} \left(1 - \frac{e\varphi_s}{W_{e,h}}\right)^4} = 0.1(1 + \kappa). \quad (19)$$

Here $\kappa = \kappa(\varphi_s)$ is introduced to qualitatively take into account a possible correction of the 1-D model. In general κ depends on the surface potential φ_s . In different situations its value can vary significantly. In the 1-D case (for very strong magnetic field when ions are attached to the magnetic field lines) $\kappa = 0$. If the Larmour radius of ions is much larger than an object (e.g. dust grain), the 1-D approximation fails. The physical cross-section of a negatively charged dust grain is larger than its geometric cross-section due to the attraction of positively charged ions, and κ tends to a well-known value $\kappa \approx -\frac{e\varphi_s}{T_{th}}$. In a strong magnetic field the transverse drift of ions (which causes the

deviation from the 1-D model) should be small enough. In this case we expect only a small deviation from the 1-D model. The first term in eq. (19) is the difference between the fluxes of thermal primary electrons and the secondary electrons generated by these primaries. The next term describes the flux of energetic electrons. The last term on the left-hand side corresponds to the contribution of secondary electrons generated by energetic electrons from the radiation belt. The right-hand side gives the input of thermal and energetic ions. Analysis of this equation shows that the surface potential is determined by energetic electrons and not by thermal electrons while $0.1(1 + \kappa) < 2.8$. The role of the secondary electrons produced by energetic electrons hitting the surface is negligible compared to all other fluxes that determine the surface potential, see eq. (19). Nevertheless the flux of these electrons at the surface is finite and it still plays a significant role in high charging of some dust grains on the surface of the moon (the mechanism suggested by Wang et al., 2016). The absolute value of this potential

$$|e\varphi_s| \approx \left(\frac{28}{1 + \kappa} - 1 \right) W_{e,h} \quad (20)$$

is very high, e.g. $e\varphi_s \approx -2.1$ MeV, if we take $\kappa = 1$. Such a high value of the surface potential is determined first of all by the magnitude of the flux of energetic electrons. The stronger this flux the higher is the absolute value of the surface potential. This is in accordance with the laboratory experiments by Wang et al. (2016) where it is shown that "when the energy of electrons was increased gradually to 120 eV, the surface potential simply followed to be increasingly negative, reaching ~ 120 V...". A somewhat similar situation occurs in the shadow of the Earth Moon when solar energetic particles (SEP) reach the vicinity of our planet. In the SEP event the estimated potential of the Moon's surface in the shadow grows many times (up to -4000 V) compared to the usual situation, see e.g. Halekas et al. (2007). The second factor that influences the magnitude of the surface potential is the distribution function of the energetic electrons. To demonstrate this we introduce another model loss-cone distribution which decreases stronger for high energies of electrons than the first loss-cone distribution given by eq. (4)

$$F_e^{(h)} = \frac{48}{\pi^2} N_{e,h} \frac{v_{\perp}^2 V_{e,h}^5}{(v_z^2 + v_{\perp}^2 + V_{e,h}^2)^5}. \quad (21)$$

After the substitution of the corresponding flux of energetic electrons into eq. (19) we find the electric potential on the surface of Thebe:

$$|e\varphi_s| \approx \left(\sqrt{\frac{53}{1 + \kappa}} - 1 \right) W_{e,h}. \quad (22)$$

The obtained potential is smaller than the previous one given by eq. (20) (approximately 2.5 times for $\kappa = 1$), that is $e\varphi_s \approx -800$ KeV. Note that the suggested two loss-cone distributions decrease with the growth of the electron energy somewhat similar to the kappa distribution introduced earlier (Divine and Garrett, 1983). The

equation describing the surface potential at the polar region of Amalthea is slightly different because the flux of energetic electrons in the vicinity of Amalthea is smaller. The corresponding equation takes the form:

$$(12 - 5.3\delta_m) \exp\left(\frac{e\varphi_s}{T_{th}}\right) + \frac{0.2}{1 - \frac{e\varphi_s}{W_{e,h}}} = 0.09(1 + \kappa). \quad (23)$$

In eq. (23) we have neglected a small contribution of secondary electrons produced by energetic primaries. The approximate solution of eq. (23) for small enough $\kappa \leq 1$ is:

$$|e\varphi_s| \approx \left(\frac{2.2}{1 + \kappa} - 1\right) W_{e,h}. \quad (24)$$

The solution of eq. (24) corresponds to a smaller surface electric potential compared to eq. (20). Taking $\kappa = 0.7$ we obtain the surface potential $e\varphi_s = -49$ KeV. It should be mentioned that with the growth of the flux of ions the absolute value of the surface potential rapidly decreases and the contribution of thermal electrons to the total flux increases. The fluxes of thermal and energetic electrons become equal at $e\varphi_s \approx -161$ eV (for $\delta_m = 1, \kappa \approx 3$). If the flux of ions continues to grow, thermal electrons begin to determine the electric potential on the surface:

$$e\varphi_s \approx T_{th} \ln\left(\frac{0.09(1 + \kappa) - 0.2}{12 - 5.3\delta_m}\right). \quad (25)$$

Such a transition from a very strong surface potential (eq. 24) to a smaller one (eq. 25) is more probable in case of Amalthea than in case of Thebe.

5 Electric fields above the surfaces of Thebe and Amalthea

The aim of this section is to give analytical estimates of the electric fields above Thebe and Amalthea in their polar regions. The procedure is straightforward. We need to substitute concentrations of electrons and ions (found from their distribution functions) into the Poisson equation:

$$\frac{d^2\varphi}{dz^2} = 4\pi e \left(N_i^{(th)}(\varphi) + N_i^{(h)}(\varphi) - N_e^{(th)}(\varphi) - N_e^{(h)}(\varphi) - N_e^{(sec)}(\varphi) \right). \quad (26)$$

Here, $N_i^{(th)}$ and $N_i^{(h)}$ are the concentrations of thermal and energetic ions above the surface at some height z , $N_e^{(th)}$ is the concentration of thermal electrons at the height z which consists of electrons reaching the surface and which are reflected by a strong electric potential below a given height, $N_e^{(h)}$ is the concentration of energetic electrons, and $N_e^{(sec)}$ is the concentration of secondary electrons created at the surface of the moon.

Eq. (26) should be solved with the boundary conditions at the surface $\varphi(z=0) = \varphi_s$ and very far above the surface $\varphi(z=\infty) = 0$. Unfortunately, even in the 1-D case this equation can be solved only numerically. Nevertheless, it is possible to give reliable estimates of the distribution of the electric potential above the surface in analytical form.

Again we assume that the deviation from the 1-D case in the motion of ions just above the surface is small. In this case the electric potential in the polar region of Thebe is given by eq. (20), and for Amalthea by eq. (24). Note that far above the surface the quasi-neutrality in the 1-D case cannot be supported. Indeed, all ions approaching from above along the field line are absorbed by the surface while almost all thermal electrons are reflected by a strong negative potential. At the same time ions coming from below in the 1-D case are screened by the moon and hence cannot contribute to quasi-neutrality. In order to obtain quasi-neutrality of the plasma we need to consider that the magnetosphere of Jupiter moves with the rotation of Jupiter which is faster than the orbital velocity of Thebe or Amalthea. Due to this, ions coming from below along the magnetic field lines contribute to the restoration of quasi-neutrality in the plasma far above the moon's surface.

We would like to find analytically the vertical electric field above the surface. For this aim we shall use a slightly modified procedure suggested by Borisov and Mall (2006). Estimates show that for strong surface potentials the main contribution to the left-hand side of the Poisson equation (26) just above the surface gives the concentration of thermal ions. Therefore, we proceed with the following approximate equation:

$$\frac{d^2F}{dz^2} \approx \frac{1}{2R_D^2} \frac{1}{\sqrt{\pi F(z)}}. \quad (27)$$

Here $F = -\frac{e\varphi}{T_{th}}$, $R_D = V_{e,th}/\omega_{Pe}$ is the Debye radius, $\omega_{Pe} = \left(\frac{4\pi e^2 N_0}{m}\right)^{1/2}$ is the plasma frequency of thermal electrons. Multiplying both sides with dF/dz and integrating with respect to z we find:

$$\frac{dF}{dz} = -\frac{1}{R_D} \left(\frac{2}{\sqrt{\pi}} (C_0 + \sqrt{F}) \right)^{1/2}, \quad (28)$$

where C_0 is an unknown constant. Assuming that the absolute value of C_0 is much less than the dimensionless potential $F_s = -\frac{e\varphi_s}{T_{th}}$ on the surface of the moon (for details see Borisov and Mall, 2006), we find an approximate value for the potential F above the surface in the polar region:

$$F \approx F_s - \frac{\sqrt{2}}{\pi^{1/4}} F_s^{1/4} \frac{z}{R_D}. \quad (29)$$

Potentials F_s for Thebe and Amalthea can be found from eq. (20) and eq. (24) respectively. Assuming as an example that for Thebe $\kappa = 1$, we find that $e\varphi_s \approx -2.1$ MeV. Now we can estimate the electric field just above the surface of Thebe:

$$\frac{d\varphi}{dz} \approx \frac{T_{th}}{eR_D} \frac{2^{1/2}}{\pi^{1/4}} F_s^{1/4}. \quad (30)$$

It follows from eq. (30) that the electric field $E_z(0)$ depends on the surface potential weakly enough $\propto F_s^{1/4}$. For Thebe if the surface potential is $e\varphi_s \approx -2.1$ MeV, the electric field is estimated as $E_s \approx -0.71$ V cm⁻¹.

Similarly, we can find the electric field at the surface of Amalthea. Assuming for example that $\kappa = 0.7$ we find from eq. (24) that the surface potential for Amalthea is $e\varphi_s \approx -49$ KeV and the surface electric field is $E_s \approx -0.39$ V cm⁻¹. Thus, even though the negative potential on the surface is very strong (especially for Thebe), the electric field is quite moderate. The electric field slowly decreases with the height above the surface according to eq. (28). This decrease can be expressed in an explicit form:

$$|eE_z| \approx \frac{T_{th}}{R_D} F_s^{1/4} \left(1 - \frac{0.25}{F_s^{3/4}} \frac{z}{R_D} \right). \quad (31)$$

It follows from eq. (31) that this decrease at some distance above the surface (while the constant C_0 in eq. (28) can be neglected) is very weak. The characteristic scale is of the order of $\Delta z \sim R_D F_s^{3/4}$. With the help of these estimates lofting of charged dust grains above the surface of Thebe and Amalthea will be discussed in Section 7.

6 Action of adhesion force and multiple electric charges on dust grains

It is well-known that the adhesion force and gravity can prevent the lofting of dust grains from the surface of a cosmic body. The magnitude of the adhesion force between dust grains lying on the surface as a function of size was discussed in many publications, see, e.g. Hartzell and Scheeres (2011); Hartzell et al. (2013); Hartzell and Scheeres (2013); Kimura et al. (2014); Cooper et al. (2001) and references therein. According to the theory the adhesion force between dust grains depends on their contact area and material of grains (also the surface chemistry is important). Theoretical estimates show that the adhesion force is large and to overcome it, strong electric fields are required. For example, for micron size grains according to Hartzell and Scheeres (2011); Kimura et al. (2014) the electric field should exceed $10^2 - 10^3$ V cm⁻¹ and even more. Note that for irregular grains according to Cooper et al. (2001) the adhesion force varies by several orders of magnitude. Thus, significant uncertainty in the magnitude of this force should be taken into account.

Several different ideas were introduced to explain how such electric fields can be formed at the surface of a cosmic body. It was argued by Criswell (1973); Rennilson and Criswell (1974); De and Criswell (1977) that near the terminator on a flat surface strong electric fields can appear between two points if one of them is exposed to the solar UV radiation and the other point is in shadow. Later on it was shown theoretically that at the terminator and in the shadow the roughness of the surface can help the formation of strong electric fields. Indeed, according to Borisov and Mall (2006) non-equal charging of two different slopes of a small cavity (or a hill) by the solar wind electrons and protons can produce significant local electric fields. Recently it was

demonstrated in a laboratory experiment by Wang et al. (2016) that in the presence of thermal plasma the action of the electron beam on a rough porous surface can create very strong electric charges on some dust grains (much larger than one elementary charge) due to the secondary electron emission. In such a case sub-micron and micron size grains begin to move on the surface. According to estimates presented by Wang et al. (2016); Schwan et al. (2017) dust grains lofted from the surface have electric charges orders of magnitude higher than the elementary charge. This experimental result, despite some constraints in the explanation (positive electric charges should be taken into account), provides the most convincing argument that charged dust grains lying on the surface can overcome the adhesion force.

Therefore, due to bombardment by energetic charged particles, two types of electric fields can be singled out in the vicinity of the rough surface of a porous cosmic body. One of them is strong local electric fields that appear because energetic electrons and ions penetrating into the body produce significant additional ionization. This process results in positive charging of ionized atoms and emission of secondary electrons. Note that positive and negative electric charges are distributed stochastically on dust grains in the surface layer. According to the experiment mentioned above the electric force acting on some of the grains possibly exceeds the adhesion force and liberates such grains. The second electric field is a large-scale one acting in the plasma sheath above the surface. This regular electric field is much smaller than the typical local field and can be estimated by integration of the Maxwell equation $\nabla \mathbf{E} = 4\pi \rho_e$ (ρ_e is the electric density) across the layer where electric charges are concentrated: $E_z(+0) - E_z(-0) = 4\pi \int \rho_e(z_1) dz_1$, where $E_z(+0)$ is the vertical component of the electric field just above the surface and $E_z(-0)$ is the vertical component of the electric field below the surface layer. Note that the amount of positive electric charges that appear in the surface layer of the cosmic body due to ionization of atoms should be equal to the negative charges of the liberated secondary electrons (assuming that all these electrons remain inside the cosmic body attached to dust grains). In such a case the electric field in the plasma sheath above the surface $E_z(+0)$ is connected with the excess of negative charges on the surface produced by the fluxes of charged particles hitting the surface. Only this field determines the dynamics of charged dust particles above the surface. In the next section we will discuss the motion of charged dust grains in the plasma sheath under the action of the electric forces and gravity.

7 Lofting of dust grains in the polar regions of Thebe and Amalthea

As it was mentioned in the Introduction the lofting of charged dust grains in the electric fields above the surface of the Moon and asteroids has been discussed in many publications. As for Jupiter's moons, so far only one mechanism (micrometeoroid impacts) was considered as a source of dust above the surface. In this section we shall investigate the lofting in the polar regions of Thebe and Amalthea of charged dust grains that are able to overcome the action of the particle adhesion. Our aim is to check if the lofting of charged dust grains in the polar regions of Thebe and Amalthea

can exceed the escape velocities in the electric fields.

The equations describing the lofting of charged dust grains above the surface are:

$$\begin{aligned} M_d \frac{d^2 z}{dt^2} &= Q_d(t) E_z(z) - g_m(z) M_d \\ \frac{dQ_d}{dt} &= e \sigma_d [P_i(\varphi(z)) - P_e(\varphi(z)) + P_{uv}]. \end{aligned} \quad (32)$$

Here $M_d \approx 4\pi\rho_d a^3/3$ is the mass of a dust grain, a and ρ_d are its radius and its density, $g_m(z)$ is the gravity, $g_m(z) = g_m(0) \frac{R_m^2}{z^2 + R_m^2}$, $g_m(0)$ is the gravity on the surface of the moon, R_m is the radius of the moon, $E_z(z)$ is the electric field above the surface that changes according to eq. (31), Q_d is the electric charge on a given dust grain, σ_d is the cross-section of a dust grain, P_e, P_i represent the total fluxes of electrons and ions acting on a dust grain with some potential φ at the height z . In the general case they are determined by the distributions of different components given in Section 2. The last term in eq. (32) P_{uv} is the flux of photoelectrons produced by the action of the solar UV radiation on the grain at the sunlit side (Horányi and Burns, 1991): $P_{uv} = ef$, if $\varphi < 0$, and $P_{uv} = ef \exp(-e\varphi/T_{ph})$, if $\varphi > 0$. Here $f \approx 2.5 * 10^9 \text{ cm}^{-2}\text{s}^{-1}$ for dielectrics, $T_{ph} \approx (1 - 3) \text{ eV}$ is the temperature of the emitted photoelectrons. The boundary conditions for eqs. (32) are:

$$z(0) = 0, \quad dz/dt|_0 = 0, \quad Q_d(0) = Q_0. \quad (33)$$

Here Q_0 is the electric charge on a dust grain lying on the surface. Note that our aim is to discuss only the initial stage of the motion of dust grains. Unfortunately, the gravities of Thebe and Amalthea are not well-known. It is accepted that for Thebe the surface gravity is $g_m \approx 1.3 \text{ cm s}^{-2}$ and for Amalthea $g_m \approx 2 \text{ cm s}^{-2}$. At the same time there are some indications that Amalthea (possibly Thebe also) is rather porous, see Anderson et al. (2005). In this case their gravity could be smaller by a factor of two ($g_m \approx 0.65 \text{ cm s}^{-2}$ for Thebe and $g_m \approx 1 \text{ cm s}^{-2}$ for Amalthea).

As it was shown in the previous section, the averaged electric density of the charged surface $\Sigma_e = \int \rho_e(z) dz$ is connected with the vertical electric field. If the surface is flat we find from this relation and equation $E_z(+0) - E_z(-0) = 4\pi\Sigma_e$, that on a given dust grain with the radius a the electric charge is $q \approx 0.5E_z(+0)a^2$. For the vertical electric fields above Thebe ($E_z = -0.71 \text{ V cm}^{-1}$) and Amalthea ($E_z = -0.39 \text{ V cm}^{-1}$) dust grains with the radius $a \leq 10 \mu\text{m}$ lying on the surface should have at maximum one elementary charge (i.e. either one electron or nothing). Note that in reality as shown in laboratory experiments (Wang et al., 2016; Schwan et al., 2017) for a porous surface layer the electric charge on a given dust grain can be 2-3 orders of magnitude higher than estimated above. These experiments clearly demonstrate that some highly charged dust grains lying on the surface overcome the short-range adhesion force. The typical velocities above the surface in the experiment by Wang et al. (2016) were approximately 0.5 m s^{-1} . We are interested in much higher velocities (of the order of the escape velocities). That is why the initial velocity in eqs. (33) is assumed to be zero.

After lofting from the surface, a dust grain with electric charge Q_0 continues to acquire a negative electric charge in the shadow because the flux of electrons above the surface exceeds the flux of ions. At the initial stage the potential on the charged grain is much smaller than the potential in space. Hence, the fluxes of electrons and ions to the surface of a grain are determined by the local electric potential in space φ given by eq. (26). The absolute value of the electric potential on a grain $\varphi_d = Q_d(t)/a$ grows in time until the flux of electrons on its surface becomes equal to the flux of ions. At the same time estimating in the shadow the flux of electrons that deposit their charge on a dust grain lofting from the surface, we need to take into account that not all electrons can be stopped by a small dust grain. For a dust grain with radius $a \sim 0.5 \mu\text{m}$ we need to take into account the fluxes of electrons with the energies $W \leq 1 \text{ keV}$. Near the surface with very strong negative potential the flux of such electrons is weak. Therefore, the electric charge on a given dust grain above the surface grows very slowly (the characteristic time can be of the order of an hour and even more, depending on the size of a grain).

First, we estimate the radius of a grain with a single charge e that can overcome the surface gravity g_m :

$$a < a_{cr} = \left(\frac{3eE_z(0)}{4\pi\rho_d g_m} \right)^{1/3}, \quad (34)$$

where ρ_d is the density of dust which we take as $\rho_d \approx 1 \text{ g cm}^{-3}$. Substituting in eq. (34) the estimates obtained above for the surface electric field, we find that for Thebe $a_{cr} = 0.47 \mu\text{m}$ or $a_{cr} = 0.59 \mu\text{m}$, respectively, depending on the surface gravity. Similarly, for Amalthea $a_{cr} = 0.418 \mu\text{m}$ or $a_{cr} = 0.52 \mu\text{m}$. As we can see from these estimates the difference between critical radii due to the uncertainty of the gravity is negligible. At the same time, as shown in the laboratory experiment (Wang et al., 2016; Schwan et al., 2017) the electric charge on a given dust grain can be much higher than a single elementary charge. In this case the critical size for lofting grows significantly. For example, if the electric charge on a dust grain is $Q = 10^2 e$ the critical sizes exceed several times the values given above.

Our aim is to estimate the dynamics of a given grain above the surface. It should be mentioned that the charged dust grain moves not only vertically but also in the horizontal plane. Due to this, after some time the grain leaves the polar region where a strong negative potential exists. Hence, to discuss the trajectories of dust grains for longer time intervals we have to add the system of equations describing the dynamics of a charged dust grain subjected to $[\mathbf{V} \times \mathbf{H}]$ electric and magnetic fields, the gravity of Jupiter, and the solar UV radiation (Horányi and Burns, 1991). This will be done in a separate paper.

Before proceeding with the numerical calculations we would like to present analytical estimates of the sizes of charged dust grains that can leave the moon (Thebe or Amalthea) in electric fields. We shall take for the escape velocity of Thebe $V_{esc} = 25 \text{ m s}^{-1}$ and the density $\rho_d = 1 \text{ g cm}^{-3}$. It follows from the conservation of energy that a dust grain with the charge $Q = 100 e$ and the radius a lofting from the surface with the potential $e\varphi_s = -2.1 \text{ MeV}$ leaves the moon if $a < 2.2 \mu\text{m}$. For smaller potential $e\varphi_s = -800 \text{ KeV}$

the size should not exceed $a = 1.6 \mu\text{m}$. For Amalthea assuming the surface potential to be $e\varphi_s = -49 \text{ KeV}$, see the end of Section 5, and the escape velocity $V_{esc} = 58 \text{ m s}^{-1}$ we find that to leave the moon, dust grains should have a size $a < 0.5 \mu\text{m}$. These estimates correspond to sizes of grains detected above Thebe and Amalthea, respectively.

Now we present the results of numerical calculations for the initial stage of dust grains lofting from Thebe and Amalthea in the shadow. We assume that some dust grain with radius a lying on a rough surface in the polar region of Thebe (or Amalthea) has a negative charge 2-3 orders of magnitude higher than in the case of a flat surface (Wang et al., 2016; Schwan et al., 2017). In our calculations we take for the surface gravity of Thebe the value $g_m(0) = 1.3 \text{ cm s}^{-2}$ and for Amalthea $g_m(0) = 2 \text{ cm s}^{-2}$. The calculations are carried out for periods when changes in the electric charge on a given dust grain can be neglected. The averaged radius of Thebe is $R_m = 49 \text{ km}$, while that of Amalthea is $R_m = 83.4 \text{ km}$, the Debye radius R_D for Thebe is $R_D \approx 10 \text{ m}$, while for Amalthea it is $R_D \approx 7.14 \text{ m}$. In Figure 1 we present the velocities of two dust grains with radii $a = 0.4 \mu\text{m}$ (continuous line) and $a = 1 \mu\text{m}$ (broken line) as functions of time. The negative electric charge on each grain is taken as $Q_0 = 100 e$. The electric field on the surface of Thebe in accordance with our estimates is $E_z(0) = 0.71 \text{ V cm}^{-1}$. The horizontal line is the escape velocity for Thebe taken as $V_{esc} = 25 \text{ m s}^{-1}$. The vertical electric field slowly decreases with the height, see eq. (31). The calculations are terminated when both grains acquire the escape velocity. Figure 2 demonstrates the growth of velocities of the same dust grains above Amalthea's surface. The electric field on the surface of Amalthea is taken as $E_z(0) = 0.39 \text{ V cm}^{-1}$. The horizontal line shows the escape velocity for Amalthea which is taken as $V_{esc} = 58 \text{ m s}^{-1}$. It is seen that a small grain above the polar region of Thebe achieves the escape velocity very quickly (in 7 sec), while for a larger grain it requires much more time (100 sec). The smaller grain above Amalthea exceeds the escape velocity in 25 sec. At the same time the larger grain does not exceed the escape velocity at all. Note that from these figures we can estimate the height above the surface at which the escape velocity is achieved. For smaller grains ($a = 0.4 \mu\text{m}$) the corresponding height above Thebe is $z_{esc}^{(Th)} \approx 87 \text{ m}$ while for Amalthea it is $z_{esc}^{(A)} \approx 750 \text{ m}$.

8 Discussion and conclusions

We have discussed the electric charging of the polar regions of Jupiter's moons Thebe and Amalthea and dust grains lofting from them. According to our analysis the lofting of charged dust grains in electric fields from the surfaces of the moons could contribute to the dust population in the gossamer rings, in addition to the main mechanism - secondary ejecta released by impacts of micrometeorites onto the surfaces. The suggested mechanism can explain some peculiarities of the dust distribution within the gossamer rings. First of all we argued that the height distribution of dust in the vicinity of Amalthea and especially for Thebe should be broader and smoother than it was modelled before. Micrometer- and sub-micrometer-sized dust grains in the vicinity of Thebe are accelerated in the electric field of the double layer and acquire a velocity sufficient to overcome the gravity of the moon. Note that in the vicinity of the moons (especially for Thebe) a rather smooth height distribution of dust was indeed detected,

see e.g. Figure 13 in Showalter et al. (2008). Thus, our results qualitatively agree with the experimental data.

According to our analysis, the polar regions of Thebe and Amalthea should have high negative potentials due to bombardment by energetic electrons. This theoretical result is based on two main assumptions. First, the electric conductivity of the moons' surfaces is assumed to be close to zero (pure insulator). Second, we expect that for the distribution of the electric potential the 1-D approximation can be used. In reality the potential significantly varies not only along the magnetic field line but also in transverse directions. But the typical velocities of the energetic and even thermal ions near the surface of the moons due to acceleration in the electric field are orders of magnitude higher than the transverse drift velocity in a strong magnetic field. Due to this, ions move more or less along the magnetic field lines. Energetic electrons that provide the main input to the charging of the surface also have longitudinal velocities much higher than the transverse drift velocity. Thus, a 1-D approximation as a first step for calculating the surface charging can be justified. The formation of strong double layers above the polar regions is an important factor that should be taken into account. These rather broad structures where the concentration of the thermal plasma is smaller than in the inner magnetosphere of Jupiter possibly can be detected by future space missions.

Acknowledgements

This work was partially performed during repeated visits of N. Borisov at MPS. NB is grateful to MPS for financial support during these visits.

References

- Anderson, J. D., Johnson, T. V., Schubert, G., Asmar, S., Jacobson, R. A., Johnston, D., Lau, E. L., Lewis, G., Moore, W. B., Taylor, A., Thomas, P. C., and Weinwurm, G. (2005). Amalthea's Density Is Less Than That of Water. *Science*, 308:1291–1293.
- Bolton, S. J. (2010). The Juno Mission. In Barbieri, C., Chakrabarti, S., Coradini, M., and Lazzarin, M., editors, *Galileo's Medicean Moons: Their Impact on 400 Years of Discovery*, volume 269 of *IAU Symposium*, pages 92–100.
- Borisov, N. and Mall, U. (2006). Charging and motion of dust grains near the terminator of the moon. *Planetary and Space Science*, 54:572–580.
- Burns, J. A. (1984). Planetary rings. *Advances in Space Research*, 4:121–134.
- Burns, J. A., Simonelli, D. P., Showalter, M. R., Hamilton, D. P., C., P. C., and Esposito, L. W. (2004). *Jupiter's Ring-Moon System*, pages 241–262. Jupiter. The planet, satellites and magnetosphere. Edited by Fran Bagenal, Timothy E. Dowling, William B. McKinnon. Cambridge planetary science, Vol. 1, Cambridge, UK: Cambridge University Press, ISBN 0-521-81808-7, 2004.

- Colwell, J. E., Gulbis, A. A. S., Horányi, M., and Robertson, S. (2005). Dust transport in photoelectron layers and the formation of dust ponds on Eros. *Icarus*, 175:159–169.
- Cooper, K., Gupta, A., and Beaudin, S. (2001). Simulation of the adhesion of particles to surfaces. *J. Colloid and Interface Science*, 234:284–292.
- Criswell, D. R. (1973). Photoelectrons and Solar Wind/Lunar Limb Interaction. *Moon*, 7:202–238.
- De, B. R. and Criswell, D. R. (1977). Intense localized photoelectric charging in the lunar sunset terminator region, 1. Development of potentials and fields. *Journal of Geophysical Research*, 82:999.
- de Pater, I., Showalter, M. R., Burns, J. A., Nicholson, P. D., Liu, M. C., Hamilton, D. P., and Graham, J. R. (1999). Keck Infrared Observations of Jupiter’s Ring System near Earth’s 1997 Ring Plane Crossing. *Icarus*, 138:214–223.
- de Pater, I., Showalter, M. R., and Macintosh, B. (2008). Keck observations of the 2002 – 2003 jovian ring plane crossing. *Icarus*, 195:348–360.
- Dikarev, V., Krivov, A., and E., G. (2006). Two stages of dust delivery from satellites to planetary rings. *Planetary and Space Science*, 54:1014–1023.
- Divine, N. and Garrett, H. B. (1983). Charged particle distributions in Jupiter’s magnetosphere. *Journal of Geophysical Research*, 88:6889–6903.
- Garrett, H. B., Levin, S. M., Bolton, S. J., Evans, R. W., and Bhattacharya, B. (2005). A revised model of Jupiter’s inner electron belts: Updating the Divine radiation model. *Geophysical Research Letters*, 32:L04104.
- Graps, A. L., Jones, G. H., Juhász, A., Horányi, M., and Havnes, O. (2008). The charging of planetary rings. *Space Science Reviews*, 137:435–453.
- Halekas, J. S., Delory, G. T., Brain, D. A., Lin, R. P., Fillingim, M. O., Lee, C. O., Mewaldt, R. A., Stubbs, T. J., Farrell, W. M., and Hudson, M. K. (2007). Extreme lunar surface charging during solar energetic particle events. *Geophysical Research Letters*, 34:L02111.
- Hartzell, C. M. and Scheeres, D. J. (2011). The role of cohesive forces in particle launching on the Moon and asteroids. *Planetary and Space Science*, 59:1758–1768.
- Hartzell, C. M. and Scheeres, D. J. (2013). Dynamics of levitating dust particles near asteroids and the Moon. *Journal of Geophysical Research*, 118:116–125.
- Hartzell, C. M., Wang, X., Scheeres, D. J., and Horányi, M. (2013). Experimental demonstration of the role of cohesion in electrostatic dust lofting. *Geophysical Research Letters*, 40:1038–1042.
- Horányi, M. (1993). Dust in planetary magnetospheres. *Advances in Space Research*, 13:231–239.

- Horányi, M. and Burns, J. A. (1991). Charged dust dynamics - Orbital resonance due to planetary shadows. *Journal of Geophysical Research*, 96:19283–19289.
- Horányi, M., Walch, B., Robertson, S., and Alexander, D. (1998). Electrostatic charging properties of Apollo 17 lunar dust. *Journal of Geophysical Research*, 103:8575–8580.
- Khurana, K. K., Kivelson, M. G., Vasyliunas, V. M., Krupp, N., Woch, J., Lagg, A., Mauk, B. H., and Kurth, W. S. (2004). *The configuration of Jupiter’s magnetosphere*, pages 593–616. Jupiter. The planet, satellites and magnetosphere. Edited by Fran Bagenal, Timothy E. Dowling, William B. McKinnon. Cambridge planetary science, Vol. 1, Cambridge, UK: Cambridge University Press, ISBN 0-521-81808-7, 2004.
- Kimura, H., Senshu, H., and Wada, K. (2014). Electrostatic lofting of dust aggregates near the terminator of airless bodies and its implication for the formation of exozodiacal disks. *Planetary and Space Science*, 100:64–72.
- Krivov, A. V., Krüger, H., Grün, E., Thiessenhusen, K.-U., and Hamilton, D. P. (2002). A tenuous dust ring of Jupiter formed by escaping ejecta from the Galilean satellites. *Journal of Geophysical Research*, 107:E1, 10.1029/2000JE001434.
- Krüger, H., Hamilton, D. P., Moissl, R., and Grün, E. (2009). Galileo in-situ dust measurements in Jupiter’s gossamer rings. *Icarus*, 203:198–213.
- Lee, P. (1996). Dust Levitation on Asteroids. *Icarus*, 124:181–194.
- Levin, S. M., Bolton, S. J., Gulkis, S. L., Klein, M. J., Bhattacharya, B., and Thorne, R. M. (2001). Modeling Jupiter’s synchrotron radiation. *Geophysical Research Letters*, 28:903–906.
- Ockert-Bell, M. E., Burns, J. A., Daubar, I. J., Thomas, P. C., Veverka, J., Belton, M. J. S., and Klaasen, K. P. (1999). The structure of Jupiter’s ring system as revealed by the Galileo imaging experiment. *Icarus*, 138:188–213.
- Owen, T., Danielsen, G. E., Cook, A. F., Hansen, C., Hall, V. L., and Duxbury, T. C. (1979). Jupiter’s rings. *Nature*, 281:442–446.
- Porco, C. C., West, R. A., McEwen, A., Del Genio, A. D., Ingersoll, A. P., Thomas, P., Squyres, S., Dones, L., Murray, C. D., Johnson, T. V., Burns, J. A., Brahic, A., Neukum, G., Veverka, J., Barbara, J. M., Denk, T., Evans, M., Ferrier, J. J., Geissler, P., Helfenstein, P., Roatsch, T., Throop, H., Tiscareno, M., and Vasavada, A. R. (2003). Cassini Imaging of Jupiter’s Atmosphere, Satellites, and Rings. *Science*, 299:1541–1547.
- Rennilson, J. J. and Criswell, D. R. (1974). Surveyor observations of lunar horizon glow. *The Moon*, 10:121–142.
- Schwan, J., Wang, X., Hsu, H.-W., Grün, E., and Horányi, M. (2017). The charge state of electrostatically transported dust on regolith surfaces. *Geophysical Research Letters*, 44:3059–3065.

- Showalter, M. R., Burns, J. A., Cuzzi, J. N., and Pollack, J. B. (1987). Jupiter's ring system - New results on structure and particle properties. *Icarus*, 69:458–498.
- Showalter, M. R., Cheng, A. F., Weaver, H. A., Stern, S. A., Spencer, J. R., Throop, H. B., Birath, E. M., Rose, D., and Moore, J. M. (2007). Clump Detections and Limits on Moons in Jupiter's Ring System. *Science*, 318:232.
- Showalter, M. R., de Pater, I., Verbanac, G., Hamilton, D. P., and Burns, J. A. (2008). Properties and Dynamics of Jupiter's Gossamer Rings from Galileo, Voyager, Hubble and Keck Images. *Icarus*, 195:361–377.
- Smith, B. A., Soderblom, L. A., Johnson, T. V., Ingersoll, A. P., Collins, S. A., Shoemaker, E. M., Hunt, G. E., Masursky, H., Carr, M. H., Davies, M. E., Cook, A. F., Boyce, J. M., Owen, T., Danielson, G. E., Sagan, C., Beebe, R. F., Veverka, J., McCauley, J. F., Strom, R. G., Morrison, D., Briggs, G. A., and Suomi, V. E. (1979). The Jupiter system through the eyes of Voyager 1. *Science*, 204:951–957.
- Throop, H. B., Showalter, M. R., Dones, H. C. L., Hamilton, D. P., Weaver, H. A., Cheng, A. F., Stern, S. A., Young, L., Olkin, C. B., and New Horizons Science Team (2016). New Horizons Imaging of Jupiter's Main Ring. In *AAS/Division for Planetary Sciences Meeting Abstracts #48*, volume 48, page 203.01.
- Wang, X., Schwan, J., Hsu, H. W., Grün, E., and Horanyi, M. (2016). Dust charging and transport on airless planetary bodies. *Geophysical Research Letters*, 43:6103–6110.
- Whipple, E. C. (1981). Potentials of Surfaces. *Space Rev. Prog. Phys.*, 44:1197.

9 Figures

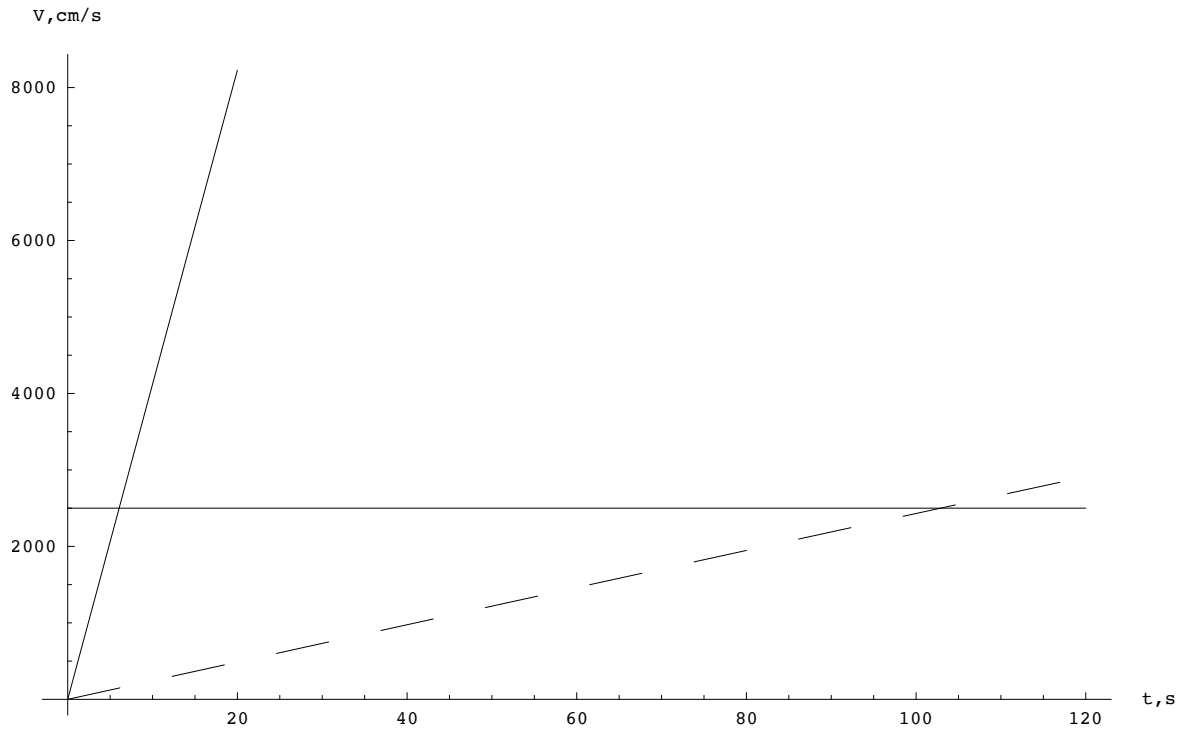


Figure 1: Vertical velocities of two dust grains with radii $a = 0.4 \mu\text{m}$ (continuous line) and $a = 1 \mu\text{m}$ (broken line) in the shadow above Thebe as a function of time. The electric charge on each grain is constant, equal to $Q = 100 e$. The gravity of Thebe is taken as $g_m \approx 1.3 \text{ cm s}^{-2}$. The horizontal line $V = 25 \text{ m s}^{-1}$ corresponds to the escape velocity of Thebe.

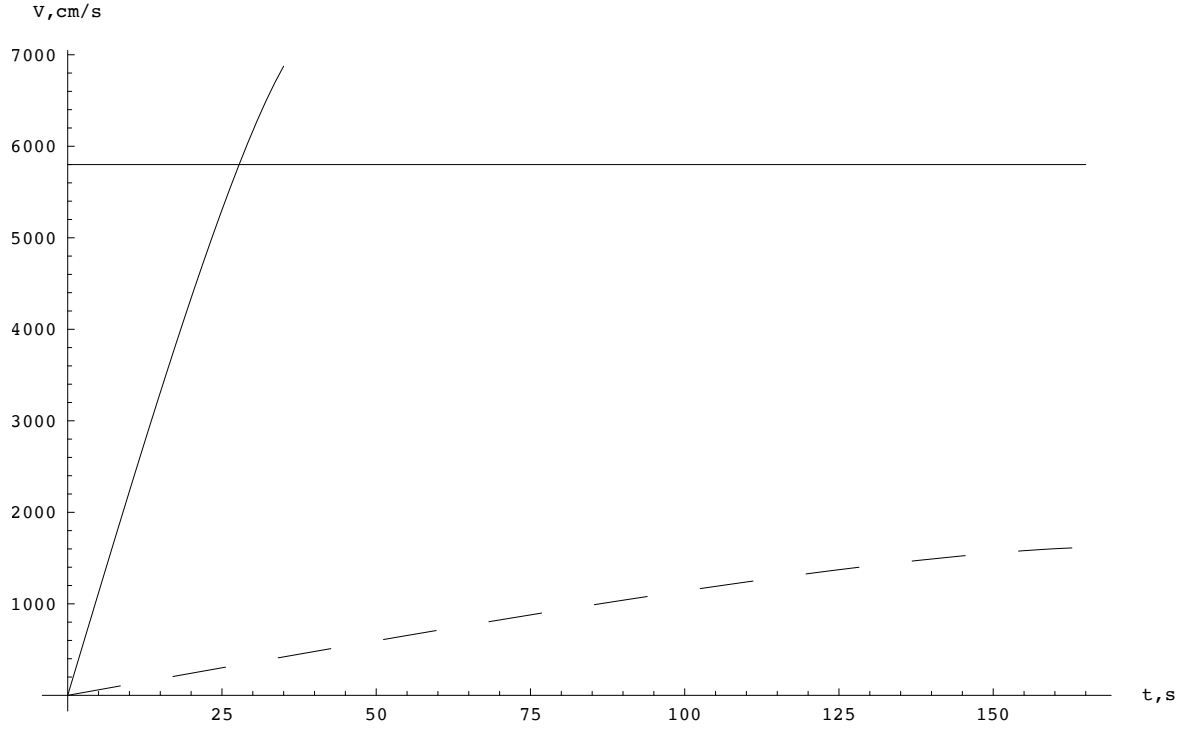


Figure 2: Vertical velocities of two dust grains with radii $a = 0.4 \mu\text{m}$ (continuous line) and $a = 1 \mu\text{m}$ (broken line) in the shadow above Amalthea as a function of time. The electric charge on each grain is constant, equal to $Q = 100 e$. The gravity of Amalthea is taken as $g_m \approx 2 \text{ cm s}^{-2}$. The horizontal line $V = 58 \text{ m s}^{-1}$ corresponds to the escape velocity of Amalthea.